Dip coating of microemulsions on hollow fibres for improved membrane filtration performance: an industrial perspective?

Chloé GUZELOT, Jean-François LAHITTE, Jean-Christophe REMIGY

Laboratoire de Génie Chimique, Université de Toulouse, CNRS, INPT, UPS, Toulouse, France

Abstract

Membrane filtration performances can be enhanced by the deposition of a selective thin layer on the surface of a porous substrate. Our simulation focus on the deposition of nanometric bicontinuous microemulsions onto hollow-fibre membranes and its polymerisation using UV modules. To that end, the laws governing the deposition of linear liquids have been extended to the study of the deposition of microemulsions. Our simulation highlights the difficulty of depositing a thin liquid coating on the fibre without causing its capillary penetration into the porosity of the substrate, due to the very low surface tension of microemulsions.

Introduction

Bicontinuous microemulsions have been investigated in the last decades to create a nanostructured highly porous thin-film on the surface of supporting flat-sheet membranes, allowing to increase the selectivity without drastically impact on the permeability of the composite membranes (Galiano, 2018). However, to the best of our knowledge little to no work has been carried out to the dip-coating of such a solution onto hollow-fibres membranes (Li, 1997). In this communication, we will perform a numerical simulation aiming to predict the coating behaviour of a microemulsion on the surface of two commercial hollow-fibre membranes, assuming the microemulsions behave as linear simple fluids. We will focus on the impact of the reservoir radius on the dynamic meniscus shape and the resulting deposition regimes. Finally, based on the presented results we will discuss the industrial prospects of microemulsion dip-coating on hollow-fibres for the manufacturing of composite hollow-fibre membranes.

Description of the dip-coating process for hollow-fibre membranes

The dip-coating process allows for the continuous deposition of uniform liquid thin-film on a cylindrical substrate and is of high interest due to its low costs compared to other processes. The liquid properties (viscosity, density, surface tension, and composition/concentration) as well as the fibre geometry and the fibre speed can be tuned to reach an aimed coating thickness. The monomer solution is then polymerised using UV or IR lamps. The dip-coating process is presented in Figure 1.

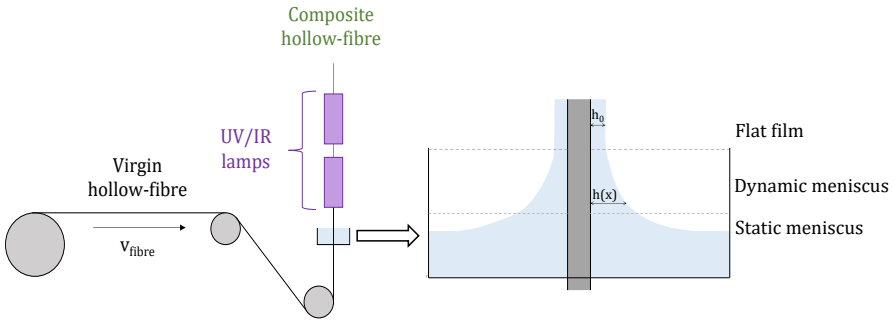

Figure 1 – Hollow-fibre membrane dip-coating photografting module and liquid meniscus representation.

The fibre dip-coating entails the motion of the cylindrical substrate through a coil and then through a liquid solution bath. This solution is drawn by the fibre and forms a thin liquid layer on the surface of the fibre. Upon removal of the fibre from the liquid solution, a meniscus is formed and three domains can be identified. The first region consists of the static meniscus and is located immediately in contact with the liquid bath, where surface tension effects dominate. The second region consists of the dynamic meniscus, where the film is starting to be drawn by the fibre. The meniscus thickness h(x) is driven by the forces applied on the liquid and governs the final film thickness deposited onto the substrate. These forces are dependent on the liquid

properties, on the geometry and speed of the substrate – which will impact on the viscous and inertia forces. The last region consists of the final and flat deposited film, which thickness is constant as only the viscous and gravitational forces are exerted on the deposited liquid.

Models for the prediction of dip-coating of linear fluids – applications to microemulsions

The laws describing the behaviour of the coating are governed by three dimensional numbers, which compare the forces applied on the fluid. The capillary number (Ca) compares the viscous forces to the capillary ones, the Weber number (We) compares inertia to capillary forces and the Bond number (Bo) the gravity to capillary forces, cf. Eq. 1 to Eq. 3.

$$\mathrm{Ca} = \frac{v_{\mathrm{fibre}}\eta}{\gamma} \quad \text{Eq. 1}$$

$$\mathrm{We} = \frac{{v_{\mathrm{fibre}}}^2 \rho r_{\mathrm{fibre}}}{\gamma} \quad \text{Eq. 2}$$

$$\mathrm{Bo} = \frac{{r_{\mathrm{fibre}}}^2 \rho g}{\gamma} = \left(\frac{r_{\mathrm{fibre}}}{l_c}\right)^2 \quad \text{Eq. 3}$$

Where γ, η and ρ are respectively the surface tension ($N.m^{-1}$), the viscosity (Pa.s) and the density ($kg.m^{-2}$) of the coated liquid; v_{fibre} and r_{fibre} the wiring speed ($m.s^{-1}$) and the fibre outer radius (m), g the acceleration of gravity ($m.s^{-2}$) and l_c the capillary length (m) of the deposited liquid.

The homogeneity and the thickness h_0 of the deposited coating are governed by these three adimentional numbers and are essential for the numerical prediction of the coating behaviour. To that end, predictive laws were developed based on Landau, Levich and Derjaguin models, as presented in Table 1. It should be noted that these equations presented are valid only if the Eq. 4 to Eq. 5 are satisfied. In practice, these two equations indicate that the fibre outer radius must be strictly lower to the capillary length l_c (Eq. 4) and that the inertia is negligible compared to the capillary forces (Eq. 5).

$$\mathrm{Bo} = \left(\frac{r_{\mathrm{fibre}}}{l_c}\right)^2 \ll 1 \quad \text{Eq. 4}$$

$$\eta \ll \sqrt{\gamma \rho r_{\mathrm{fibre}}} \quad \text{Eq. 5}$$

$$l_c = \sqrt{\frac{\gamma}{\rho g}} \quad \text{Eq. 6}$$

The capillary length l_c is a length scaling factor that compares gravity to the surface tension forces, cf. Eq. 6. This parameter is one of the key factors impacting on the behaviour of the liquid meniscus and the different regimes describes above. In order to reach a homogeneous uniform liquid coating, the divergence and expulsion droplets domains are to be avoided. The five regimes described in Table 1 highlight the evolution of the forces exerted on the dynamic meniscus as it grows due to the increase in fibre velocity.

In order to predict the behaviour of our coating, some assumptions have to be made to apply the models presented. We assumed that the fibre speed limitations for emulsions (Quéré, 1998; Colosqui, 2013; Gans, 2019) do not apply to microemulsions, and more specifically to bicontinuous microemulsions. Indeed, all the phenomena and models describing the colloidal and emulsified systems coatings include the size of the suspended objects as a critical factor for the homogeneity of the system because those systems involve the entrainment of micrometric objects in a micrometric thin-film. If the coating is thinner than the suspension size, a segregation is observed. The dip-coating of concentrated emulsions also proved modification of the composition as a function of the fibre velocity, probably resulting from a shearing of the droplets in the liquid meniscus. Because microemulsions are of nanometric size, we hypothesise that the previous behaviours regarding the thickness and the composition will not occur due to the nanometric size of the dispersed objects compared to the micrometric deposited coating. We will therefore consider the microemulsions to follow the laws described in Table 1 for simple and linear liquids.

Table 1 – Dip-coating deposition regimes as a function of the liquid properties (Quéré, 1998; Quéré, 1999).

Regime description	Conditions	Predictive thickness equation	
Visco-capillary	• Ca,We << 1 • $h_0 << l_c$ Gravity neglected	$h_0^{LLD} = 1.34 l_c Ca^{\frac{2}{3}}$ *Landau-Levich-Derjaguin equation (LLD)*	Eq. 7
Visco-capillary and visco-inertial	• Ca,We < 1 • $h_0 << l_c$ Gravity neglected • $\sqrt{\gamma \rho r} > \eta$	$h_0 = \frac{1.34 r_{fibre} Ca^{\frac{2}{3}}}{1 - \beta(h_0) We}$ $\beta(h_0) = \frac{1}{5}\left(\ln\left(\frac{r_{reservoir}}{h_0}\right) - 3\right)$	Eq. 8
Saturation and initial divergence	• $\beta(h_0) \to 0$ • $h_0 > r$ • $h_0 > \frac{r_{reservoir}}{\exp(3)}$	$h_0 = \frac{r_{reservoir}}{\exp(3)}$	Eq. 9
Viscous boundary – Lower fibre speed	• We~1 Layer enclosing the dynamic meniscus Neglected capillary suction • $h_0 < \sqrt{\frac{\eta h_{reservoir}}{\rho v_{fibre}}}$	$h_0 \sim \sqrt{\frac{\eta h_{reservoir}}{\rho v_{fibre}}}$	Eq. 10
Viscous boundary – Higher fibre speed	• We >> 1 No more capillary action: dragging of the layer set in motion by the fibre • $h_0 \geq \sqrt{\frac{\eta h_{reservoir}}{\rho v_{fibre}}}$	$h_0 = \alpha \sqrt{\frac{\eta h_{reservoir}}{\rho v_{fibre}}}$ α a constant (thickening factor)	Eq. 11
Expulsion droplets	• $L > L^* = \frac{r_{reservoir}}{Ca}$	Irregular and uncontrolled coating	

Simulation of hollow fibre coating - applications to microemulsions on MF-PES and UF-PS hollow-fibres

In the following simulation, two commercial hollow-fibre membranes have been considered: the Type TF10 MicroPES™ (3M – previously Membrana) and the Zeeweed™ 500S (General Electrics – previously Suez) fibres. The geometrical properties used for all the analytical determination are reported in Table 2. The MicroPES™ is a microfiltration polyethersulfone (PES) membrane, while the Zeeweed™ is an ultrafiltration hydrophilic polyvinylidene fluoride (PVDF) membrane. These two membranes were chosen to compare the coating behaviour based on the initial porosity of the substrate, but also due to their composition. Indeed, on the one hand PES allows for a photografting which is of high interest to create a permanent and strong coating on the substrate surface. On the other hand, PVDF is one of the most used polymers for the synthesis of membranes for water treatment

Table 2 – Geometric parameters of the fibres considered in this simulation.

Hollow fibre	Membrane type	Outer radius (m)	Inner radius (m)	Pore radius (m)
MicroPES™	Microfiltration (MF)	$250\ 10^{-6}$	$150\ 10^{-6}$	$0.25\ 10^{-6}$
Zeeweed™	Ultrafiltration (UF)	$800\ 10^{-6}$	$450\ 10^{-6}$	$0.036\ 10^{-6}$

The important properties of the microemulsion to be considered in the numerical simulation are also described in Table 3. The microemulsion considered is an acrylate system stabilised by non-ionic non-polymerisable commercial surfactants developed in our research team (Sanz, 2006).

Table 3 – Physico-chemical properties of the microemulsion considered in this simulation.

Density (kg.m^{-3})	Viscosity (Pa.s)	Surface tension (N.m^{-1})	Capillary length (m)
1024 ± 2	0.007 ± 0.002	0.0301 ± 0.002	1.76 10^{-3}

The results presented in Table 4 indicate that the equations presented in Table 1 can be applied, as the conditions in Eq. 4 to Eq. 6 are met. Out of those five different domains only the visco-capillary and the visco-inertial regimes will be discussed in this present work. Although the viscous boundary regime may allow for a thin, controlled and homogeneous deposit, it is however not possible to predict the thickness of the coating because the constant α can only be determined experimentally.

Table 4 – Critical numbers for the determination of the dip-coating domains for the two hollow fibre studied.

Hollow fibre	Bond number	$\sqrt{\gamma . \rho . r_{fibre}}$ (Pa.s)
MicroPES™	0.020 << 1	η << 8.1 10^{-2}
Zeeweed™	0.207 << 1	η << 15.9 10^{-2}

In order to reach the visco-capillary and the visco-inertial regimes, the capillary and Weber numbers must both be strictly lower than unity. For our simulation, we will consider the visco-capillary and visco-inertial governing equation (cf. Eq. 8) to be valid as long as the capillary and Weber numbers are below 0.9, to avoid any disruption due to the inertial divergence regime appearing when approaching $We \sim 1$. Using the physico-chemical parameters of the microemulsion listed in Table 2, the maximum fibre speed to remain in the visco-capillary domain (We < 0.9) has been established to 19.8 m.min^{-1}.

System resolution for the determination of the deposited thickness

Based on Eq. 8 and on the definition of the capillary and Weber numbers (cf. Eq. 1 and Eq. 2), a second order equation can be obtained. Using the system presented in Eq. 12 to Eq. 14, the deposited thickness can be obtained while varying both the fibre velocity and the liquid reservoir radius.

$$A . {v_{fibre}}^2 + B . {v_{fibre}}^{\frac{2}{3}} - h_0 = 0 \quad \text{Eq. 12}$$

$$A = \frac{h_0}{5}\left[\ln\left(\frac{r_{reservoir}}{h_0}\right) - 3\right] \quad \text{Eq. 13}$$

$$B = 1.34(r_{fibre} + h_0)\left(\frac{\eta}{\gamma}\right)^{\frac{2}{3}} \quad \text{Eq. 14}$$

The importance of the reservoir radius is linked to the achievable height and width of the meniscus formed during the passing of the fibre. This radius is the limiting factor to the growth of the meniscus when increasing the fibre speed. For this reason, in the present document we will refer to the wall distance between the outer surfaces of the fibre to the tank wall as the reservoir radius. The effective tank radius to be considered when designing the installation will have to include the external diameter of the hollow-fibre to accommodate the present numerical simulation. When the liquid reservoir is increased, the meniscus grows and so does the deposited thickness (Quéré, 1998). However, we do not expect the meniscus to increase indefinitely with the reservoir radius. We will therefore consider that once the maximum meniscus height is achieved, so is its maximum width. Above an upper reservoir radius boundary, a maximum $r_{reservoir}$ will be reached in Eq. 13. This upper bound was determined as $r_{reservoir} \approx 1.85 l_c = 3.3$ mm for the investigated microemulsion coating, regardless of the fibre radius (Tang, 2019). We therefore propose to study the deposited coating thickness as a function of the fibre speed for three values of the reservoir radius (excluding the fibre radius). The fibre speed range investigated was chosen so that We<0.9 (0.1 to 19.8 m.min^{-1}) and the three reservoir radii were chosen to represent the whole range between 0.1 and 3.3 mm (0.1, 1.6 and 3.3 mm). Once the Weber number exceeded 0.9 we considered the occurrence of a saturation regime. Indeed, although the viscous boundary or expulsion droplet regimes may occur, some experimental data ($h_{reservoir}$ and the thickening factor α) are needed to display the evolution of the coating thickness in such domains.

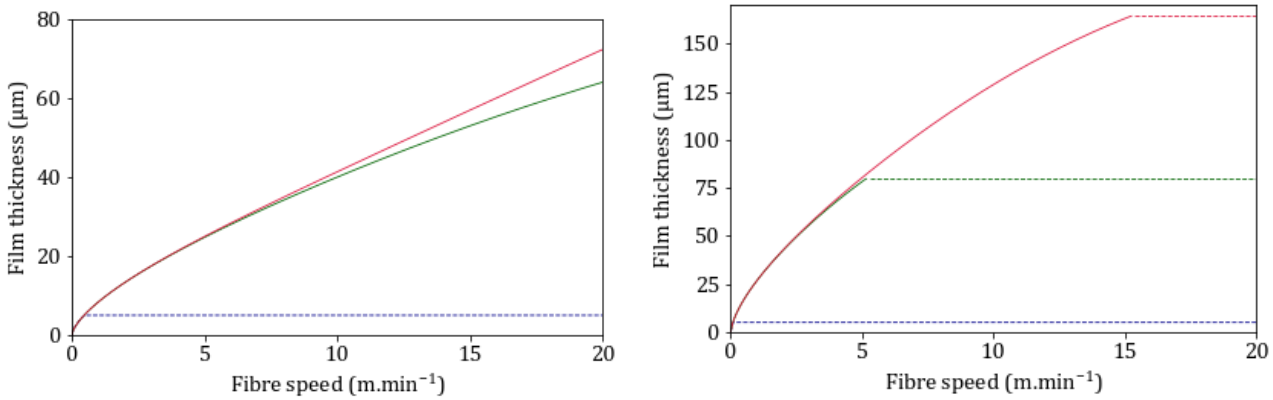

Figure 2 – Evolution of the coating thickness based on the fibre speed and the reservoir radius for the MicroPES™ (**left**) and the Zeeweed™ (**right**) hollow-fibres. The reservoir radius does not include the fibre radius. Reservoir radius of (**red**) 3.3 mm, (**green**) 1.6 mm and (**blue**) 0.1 mm. (**plain**) Visco-inertial regime and (**dashed**) saturation regime.

The thickness of the deposited coating was determined using Eq. 12 to Eq. 14, based on the physicochemical and geometrical parameters presented in Table 1 and Table 2, as presented in Figure 2. These two graphs highlight the impact of both the fibre speed and the reservoir radius, even though this last factor is usually overlooked in simulations. Decreasing the reservoir radius below the capillary length – and thus the meniscus width – leads to the apparition of a divergence and saturation regimes, which are independent of the fibre speed (cf. Eq. 9). We observe that the smaller the reservoir radius, the faster of these regimes occur. The saturation regime also appears earlier for bigger fibre radii as the deposited thickness becomes thicker than the dynamic meniscus, leading to the divergence regime. However, one must keep in mind that the thicknesses presented in our calculations for the saturation regime (dashed lines) is based on the equation Eq. 9, which approximates the real coating thickness. In order to remain in a visco-inertial domain and better control the process, a radius larger than the capillary length l_c – in our case 3.3 mm – should be used.

Coating perturbation after deposition on the fibre – Plateau-Rayleigh instability

Previous work of our research group demonstrated that the microemulsion would be completely polymerised in ca. 1.1 s using a polychromatic UVA-PRINT LE (Hoenle) UV lamp. Before its complete polymerisation, the deposited coating may undergo various destabilisation phenomena, such as dewetting or liquid penetration in the fibre pores. To experimentally ensure the continuity and the homogeneity of the coating, these phenomena domains are identified beforehand, for various fibre speeds and reservoir radii. Setting the liquid bath right below the lamp allows for the polymerisation to take place right after the fibre coating limiting the occurrence of instabilities as much as possible, as detailed in the next paragraphs.

The Plateau-Rayleigh instability, due to the fibre geometry, is one of the main problems resulting in the coating heterogeneity after the fibre dip-coating. Under the effect of the surface tension at the air-liquid interface, the film surface will create some undulations in order to decrease its surface energy. This will lead to a breakdown of the uniform into a succession of droplets forming fluid droplets on the fibre (Quéré, 1999; Lorenceau, 2006). For a cylindrical fibre, the instability appears as soon as the distance between the droplets is higher than the coating perimeter on the fibre. Hence, the deposition of a minimum coating thickness h_0^* (cf. Eq. 15) will prevent the Plateau-Rayleigh instability.

$$h_0^* \geq r_{fibre}(\sqrt{2} - 1) \qquad \text{Eq. 15}$$

Based on the formula Eq. 15, we calculated the minimum coating thickness to be deposited on the MicroPES™ and on the Zeeweed™ hollow-fibres to avoid the Plateau-Rayleigh instability: the deposited coating must be thicker than 104 µm and 331 µm respectively, which are never reached in our operating conditions. If the liquid is not solidified quickly enough, the Plateau-Rayleigh instability could therefore appear on both fibres in our investigated conditions: fibre speed range of [0.1-19.8] $m.min^{-1}$ and a reservoir radius (excluding the fibre radius) from 0.1 to 3.3 mm.

As thin-films are expected to reduce transfer resistance – and to maximise the permeability of the composite coated fibre – the coating must solidify before the duration of the instability development τ_{PR}, cf. Eq. 16.

$$\tau_{PR} = 12\frac{\eta {r_{fibre}}^4}{\gamma {h_0}^3} \quad \text{Eq. 16}$$

Based on the coating thickness determined for each fibre velocity and reservoir radius, using the equation system Eq. 12 to Eq. 14, it is possible to determine the characteristic time related to the occurrence of the Plateau-Rayleigh instability of each fibre speed and reservoir radius. If the thin film deposited on the surface of the fibre is able to polymerise before reaching this critical time τ_{PR}, then the Plateau-Rayleigh instability can be avoided. Combining these equations to Eq. 16, allows for the determination of the operating conditions avoiding the Plateau-Rayleigh instability domain on both fibres considered. The results highlight that, for a complete curing of the system of 1.1 s, Plateau-Rayleigh instability cannot be avoided for reservoir radii below 2.0 mm for the Zeeweed™ fibre. Using larger tank radii results in an avoidance of the instability for the fibre speed range above 7.0 m.min^{-1}. The coating of the MicroPES™ will be impacted by Plateau-Rayleigh instability below a reservoir radius of 0.5 mm for the entire fibre speed considered, but the instability will be prevented for fibre velocities above 4.8 m.min^{-1} for larger tank radii.

Coating perturbation after deposition on the fibre – Coating penetration and dewetting

The deposited coating may also penetrate the pore substrate after coating deposition. The Washburn equation allows for the determination of the capillary penetration of the liquid L_{cap} depending on the time spent by the liquid on the substrate surface Δt. This equation, presented in Eq. 17, is valid for a fibre pore radius strictly lower than the capillary length l_c for hydrophilic substrate, and for vertical dip-coating process because the pores are considered as horizontal capillaries.

$$L_{cap} = \sqrt{\frac{\gamma r_{pore}\cos\theta}{2\eta}\Delta t} \quad \text{Eq. 17}$$

In order to predict the pore penetration by the monomer microemulsion, we considered that the liquid was able to penetrate the substrate until its full polymer conversion, i.e. $\Delta t = 1.1$ s. We determined the contact angles between the PVDF and PSU – which we assumed to behave identically to PES – substrates and the microemulsion to be both 0° (superhydrophilic behaviour). The liquid penetration in the substrate in 1.1 s was therefore estimated to 205 µm for the Zeeweed™ and 760 µm for the MicroPES™ fibre, indicating a full MF-fibre thickness penetration. We then calculated the deposited minimum coating thickness to saturate the substrate pores in 1.1 s to be 150 and 71 µm for the Zeeweed™ and the MicroPES™ fibres respectively.

Based on the previous results, we evidenced for a fibre speed range of [0-19.8] m.min^{-1} and a reservoir radius (excluding the fibre radius) from 0.1 to 3.3 mm, that the deposited coating on the surface of the MicroPES™ is always thinner or equal to 71 µm. Therefore, all deposited liquid will penetrate into the MicroPES™ porosity in 1.1 s, before the microemulsion full polymerisation. On the contrary, the Zeeweed™ fibre exhibits thicker coatings – up to 164 µm – in the same investigated reservoir radius and fibre speed ranges. For specific operating conditions ($r_{reservoir} \geq 0.22 l_c$ = 0.4 mm; v_{fibre} = [0-19.8] m.min^{-1}) it is therefore possible for the deposited coating to be thicker than the prediction as the liquid thickness will penetrate the fibre porosity. The liquid penetration will lead to lower permeabilities, assuming that the microemulsion cures through the entire wall thickness - which we have proven for the MicroPES™ flat-sheet membrane. We will not discuss the dewetting perturbation of the coating because of the hydrophilic behaviour of the microemulsion coating on the two fibres. Indeed, no metastable dewetting will occur as the liquid film will always be thicker that this critical thickness described in Eq. 18. Plus, no unstable dewetting will occur as the predicted thickness we evidenced were always thicker than 10 nm (Noblin, 2004).

$$h_c = 2l_c \sin\left(\frac{\theta}{2}\right) = 0 \quad \text{Eq. 18}$$

Efficiency of the dip-coating process for microemulsions

One may now question the efficiency of the composite membrane – permeability and selectivity – and thus the attractiveness of this process: is the dip-coating of microemulsion on the surface of hollow-fibres a process of industrial interest? We can answer – at least partially – to this question by estimating the performances of such a composite hollow-fibre. To that end, we have to consider both the permeability and the selectivity of the composite polymer network. Our reasoning will be based on experiments done in the literature (Galiano, 2018) who investigated these two parameters as a function of the microemulsion coating thickness on flat-sheet membrane geometry.

Using a series resistance model (cf. Eq. 19), we can then estimate the permeability of the finale composite hollow-fibre membrane. Based on the manufacturer's data, the water permeability of the MicroPES™ and the Zeeweed™ membranes are respectively of 21000 and 900 $L.h^{-1}.m^{-2}.bar^{-1}$ at 25°C. Plus we assume that the permeability of our final polymer coating is identical to the permeability described by Galiano for its bicontinuous thin-film coating.

$$\frac{1}{\mathrm{Lp}_{\mathrm{composite}}} = \frac{1}{\mathrm{Lp}_{\mathrm{porous\ substrate}}} + \frac{1}{\mathrm{Lp}_{\mathrm{thin-film}}} \qquad \text{Eq. 19}$$

Based on the data the water permeability at 25°C of the composite membrane depending on the coating thickness has been simulated for the MicroPES™ and the Zeeweed™ hollow-fibres, as presented in Figure 3. The simulated permeability highlights the dramatic decrease of the water permeability above a 10 µm-thick coating, for which the water permeability falls below 30 $L.h^{-1}.m^{-2}.bar^{-1}$ for both fibres. Hence such a coating will lead to a permeability decrease of 99.9% and 97.1% for the MicroPES™ and the Zeeweed™ respectively. These results stress the importance of the coating thickness and bring to lights the irrelevance of the substrate selection based on their initial permeability, due to the really low permeability of the deposited coating which will predominantly govern the permeability decrease.

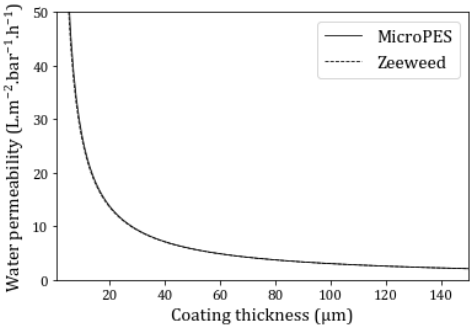

Figure 3 – Water permeability at 25°C of the composite hollow-fibres depending on the coating thickness based on the literature data obtained for a bicontinuous microemulsion.

Based on the previous results, we know that the coating will completely penetrate the MicroPES™ pores and partially the Zeeweed™ pores with a remaining continuous thin-film. The resulting permeability of such a composite membrane would be lower than 5 $L.m^{-2}.h^{-1}.bar^{-1}$ based on Galiano's work. We did not find sufficient data in the literature to perform a similar analysis regarding the selectivity of a microemulsified coating, to complete our analysis. It however appears that separative applications are not of great industrial interest, due to the low permeability of the composite membrane.

Conclusions

The well-known predictive laws of Landau-Levich-Derjaguin (LLD) for the dip-coating of a hollow-fibre membrane have been adapted in order to describe a microemulsion coating ($d_{colloid}$ < 100 nm). Our results emphasised the necessity to incorporate the reservoir radius in the coating predictive models, as the saturation regime can be obtained for speed ranges lower than expected based on the determination of the Weber number. We can therefore conclude that the divergence and saturation regimes are impacted by two independent factors: the meniscus profile (i.e. reservoir radius) and the Weber number (i.e. fibre speed).

Our work is – to our knowledge – the first aiming at the prediction of the coating thickness, homogeneity and stability for the dip-coating of a microemulsion solution on porous media. The main drawback to overcome for such mixtures is the control of pore penetration of the substrate after coating. We proved that microemulsions exhibit a superhydrophilic behaviour on both PES and PVDF substrates, thus indicating that the penetration will always be predominant and may lead to a saturation of the membrane pores. This phenomenon affects the effective coating thickness, which will be thicker than predicted by the LLD equations, leading to further reduced permeabilities. We then estimated the impact of the coating thickness based on the permeability results from Galiano's work and highlighted the need for a maximum layer thickness of 10 µm to avoid a dramatic decrease of the composite hollow-fibres permeability, for both the MicroPES™ and the Zeeweed™ supports. Such a thickness is not achievable without allowing the occurrence of the Plateau-Rayleigh instability, leading to heterogeneous coatings. As a result, coating of microemulsions on hollow-fibres using the dip-coating process is not of high interest for separative applications due to the low achievable permeabilities but might still be of interest for other applications, such as catalysis.

Plus, it remains uncertain whether the liquid would homogeneously penetrate the pores, allowing for increased selectivity over the entire surface of the fibre. Otherwise, defects would appear, resulting in a drastic reduction in permeability without increasing the selectivity (Quezada, 2007). Our simulation therefore indicates a poor suitability of the process for the desired microemulsion thickness, no matter the initial substrate permeability, pore radii and fibre radii. If our investigation exclusively focused on the visco-capillary and visco-inertial coating domains, it however seems unlikely that the viscous boundary regime might solve this problem as the main drawback to overcome is the capillary penetration of the monomer coating into the substrate porosity. We also concluded that using other coating processes (e.g. spray coating) will not be beneficial due to the nature of the monomer microemulsion penetration difficulty.

References

Colosqui C.E. ; Morris J. F.; Stone H. A., Hydrodynamically driven colloidal assembly in dip coating, *Phys. Rev. Lett.*, 2013, 110 (18), 1–5.

Galiano F.; Schmidt A.; Ye X.; Kumar R.; Mancuso R.; Curcio E.; Gabriele B.; Hoinkis J.; Figoli A., UV-LED induced bicontinuous microemulsions polymerisation for surface modification of commercial membranes – Enhancing the antifouling properties, *Sep. Purif. Technol.*, 2018, 194, 149–160.

Gans A.; Dressaire E.; Colnet B.; Saingier G.; Bazant M.Z.; Sauret A., Dip-coating of suspensions, *Soft Matter*, 2019, 15 (2), 252–261.

Li T.D., Gan L.M., Chew C.H., Teo W.K., Gan L.H., Hollow-fiber membranes coated with polymerizable bicontinuous microemulsions, *Journal of Membrane Science*, 1997, 133(2), 177-187.

Lorenceau E.; Senden T.; Quéré D., Wetting of fibers, *Molecular Gels: Materials with Self-Assembled Fibrillar Networks*, 2006, pp. 223–237.

Noblin X., Mouillage et démouillage inertiel : triplons , flaques vibrées , ondes de chocs, PhD thesis, Université Paris 6, 2004.

Quéré D., Fluid Coating on a Fiber, *Annu. Rev. Fluid Mech.*, 1999, 31 (1), 347–384.

Quéré D.; De Ryck A., Hydrodynamic coating of a fiber, *Ann. Phys. (Paris).*,1998, 23 (1), 1+.

Quezada Jiménez M. L., Photo-greffage de membranes et distributuion initiale de taille des pores : Mise en évidence des limitations, PhD thesis, Université Toulouse 3 Paul Sabatier, 2007.

Sanz F. J. E.; Lahitte J. F.; Remigy J. C., Membrane synthesis by microemulsion polymerisation stabilised by commercial non-ionic surfactants, *Desalination*, 2006, 199 (1–3), 127–129.

Tang Y.; Cheng S.; The meniscus on the outside of a circular cylinder: From microscopic to macroscopic scales, J. Colloid Interface Sci., 2019, 533, 401–408.